On the More Complex Wavelength Dependency of Airy Isostasy in Icy Shells of Ocean Worlds

Wesley S. Tucker[1] and Andrew J. Dombard[1]

[1]Department of Earth and Environmental Sciences, University of Illinois Chicago, Chicago, IL

Corresponding author: Wesley Tucker (wtucke5@uic.edu)

Key Points:

- Distinct behaviors emerge in support of icy shell topography at varying spatial scales.
- Ice shell thickness estimates using Airy isostasy are valid at only long wavelengths.

Abstract

The topography of ocean worlds is often used to infer ice shell thicknesses by assuming topography is compensated by a basal root. We systematically test the stability of isostatically compensated topography in ice shells. At short horizontal wavelengths, lithospheric strength can support surface topography, while at long wavelengths, buoyancy forces can support topography at the surface and base of the ice shell over geologic time scales. These behaviors are also seen for Airy isostasy in terrestrial worlds. Contrastingly at intermediate scales, the mechanically weak lower ice shell can inhibit the transfer of buoyancy forces to the surface. Factors such as surface temperature can alter the contribution of lithospheric strength, decreasing the stability of a compensating root. This nuanced understanding of icy shell lithospheres provides crucial insights for interpreting surface features and inferring underlying ice shell thickness, with substantial relevance for upcoming space missions to the Jovian system.

Plain Language Summary

Ocean moons have topography on their surfaces that can be used to estimate the thickness of the capping ice shells. In contrast to rocky worlds, the nature of ice shells prevents traditional approaches from being applied. In this study, we use geophysical models to simulate how topography evolves over geologic time. For small features, the stiffness of the ice crust plays a significant role in supporting topography. For larger features, buoyancy forces, like how an iceberg floats, keep topography stable over long periods. In the lower shell near the underlying ocean, the ice is near its melting temperature, which makes it much weaker than the ice nearer the surface. This weakness can prevent the buoyancy forces from reaching the surface for intermediate scale features. Understanding the dynamics of Airy isostasy in ocean worlds can help interpret data collected from space missions, and further our understanding of these icy satellites.

1 Introduction

Topography on terrestrial bodies is generally supported by a combination of factors. These include variations in crustal thickness, known as Airy isostasy (Airy, 1855), variations in density, referred to as Pratt isostasy (Pratt, 1855), and the strength of the lithosphere (Turcotte et al., 1981). The extent to which lithospheric strength contributes to topographic support depends on the wavelength of the topography (e.g., Turcotte & Schubert, 2014). For instance, at short wavelengths, the lithosphere can fully support the topographic load, analogous to a bookshelf supporting a single book. However, at sufficiently long wavelengths, the rigidity of the lithosphere is reduced, similar to many books on a sagging bookshelf. In this case, the topography is compensated by isostasy.

The concept of surface topography being compensated by an opposing basal topography (i.e., Airy isostasy) is simple and appealing. It enables interpretation of gravity and topography data collected by spacecraft using only an *a priori* knowledge of density. Consequently,

researchers have widely used this concept to estimate variations in the thickness of icy shells on ocean worlds within the Jovian and Saturnian systems.

These icy satellites display a diverse array of topographic features at various horizontal wavelengths. In addition to its use with gravity measurements, Airy isostasy has been used to estimate ice shell thickness from observations of surface features and their respective topographies. Shell thickness estimates are commonly derived from long-wavelength topography (e.g., Čadek et al., 2019b; Nimmo et al., 2011; Schenk & McKinnon, 2009), and is often used as an explanation for unexpected topography observations. For example, the unexpectedly large amplitude of Titan's long-wavelength topography may be explained, in part, by isostatic compensation (Nimmo & Bills, 2010). Estimates based on long-wavelength variations shell thickness assume that the shell is in a constant state of equilibrium. Effectively, ice flow at the base of the ice shell, driven by horizontal pressure differences, is faster than the rate of relaxation resulting in a constant compensation (e.g., Ojakangas & Stevenson, 1989; Stevenson, 2000).

Short-wavelength features are strewn across icy, ocean worlds. Europa's surface is most notably characterized by intersecting ridges that can extend for more than 1000 km with a relief of ~200 m (e.g., Pappalardo et al., 1999; Prockter & Patterson, 2009). Additionally, dark bands on Europa can rise up to 150 m above the surrounding terrain and span several tens of kilometers across (Nimmo et al., 2003b). Although linear features are ubiquitous on Europa, there are also small pits and uplifts with average diameters of around 5 km. Singer et al. (2021) employed a basic Airy isostasy model to estimate a minimum shell thickness for Europa of about 3-8 km, based on the size of these small pits. However, if sufficiently thick, the ice shell likely has the rigidity to support short-wavelength features (e.g., Nimmo et al., 2003a).

Ice shell thickness estimates have also been derived from chaos terrain on Europa. Williams & Greeley (1998) estimated a minimum thickness of just 0.2-3 km at Conamara Chaos, based on the interpretation that the blocks of the chaos terrain were floating in a liquid at the time of formation. In addition to the short-wavelength topography that is the icy blocks sitting in a matrix, chaos terrain can have their own longer wavelength topographic signature suggesting a compensated state (e.g., Schmidt et al., 2011).

Recently, efforts have been made to refine Airy isostasy for use on ice shells, specifically at low spherical harmonic degrees (see Beuthe 2021a, 2021b for an extensive review).

Hemingway and Matsuyama (2017) argued that the traditional form of Airy isostasy, in which columns of equal width contain equal mass, is not applicable when using spherical geometry as it causes lateral pressure gradients. The authors proposed an approach that assumes continuous pressure along a solid crust-mantle boundary. Čadek et al. (2019a) assessed the accuracy of these two approaches, and an "equal stress approach" proposed by Dahlen (1982), to a numerical solution of viscous flow in the crust. The authors concluded that the equal pressure approach may lead to inaccurate estimates of shell thickness for spherical harmonic degrees $l \leq 10$ when assuming a constant viscosity. When viscosity of the ice was temperature dependent, all models lost accuracy with increasing spherical harmonic degrees.

A few researchers have presented models that aimed to explain the support mechanism for observed features on the surface of icy, ocean worlds such has the plateaus on Titan (Schurmeier et al., 2016) and the megadome on Ganymede (Kay et al., 2018). For both instances, buoyancy forces were not transferred to the surface, which caused the topography at the surface and at the base of the shell to relax away. The megadome on Ganymede was found to be stable over geologic times only when Pratt isostasy was the assumed mechanism of support. On Titan, the plateaus could not be sustained via Airy isostasy, which implies that these features are unlikely to be the result of crustal thickening.

Inherent to the nature of icy shells is the mechanical weakness near the ice-ocean interface. In principle, a material near its melting point (i.e., the lower ice shell) should be limited in its ability to transfer buoyancy stress to support surface topography. This characteristic injects a level of complexity into the understanding of icy shell topographies and the mechanisms that give rise to their support. In this paper, we explore the mechanics of buoyantly supported topography from short wavelength to hemispheric wavelength scales. With upcoming spacecraft missions such as NASA's Europa Clipper, understanding the dynamics of ice shells is crucial for providing a foundation for interpreting the trove of data that could profoundly alter our knowledge of icy, ocean worlds.

2 Methods

2.1 Finite element simulations

We use the commercially available Hexagon Marc finite element package to test systematically for buoyant support of topography in icy shells. The software is well vetted for

investigations of lithospheres of icy shells (e.g., Damptz & Dombard, 2011; Dombard & McKinnon, 2002, 2006a; Kay & Dombard, 2018). The code simulates Maxwell viscoelasticity, capturing the behavior of geologic materials at both short and long timescales, (and can include plasticity as a continuum approximation for brittle failure at large stresses). We test for buoyant support of topography for wavelengths λ = 10 km up to hemispherical scales (i.e., spherical harmonic degree l = 2), increasing logarithmically. Although applicable for all icy-ocean worlds, we use Europa to guide selection of model parameters. The full finite element simulation is comprised of two steps. A thermal simulation is run to determine the temperature structure, and the results of the thermal simulation are used in the mechanical simulation.

2.2 Mesh and boundary conditions

We utilize planar half space meshes split into two layers: an outer ice shell, ostensibly 20 km thick (e.g., Billings & Kattenhorn, 2005; Hussmann et al., 2002), and an ocean with a boundary far enough away to not affect the solution (Figure 1). For short wavelengths, the ocean mesh layer is ~2.5 times the wavelength. For long wavelengths ($l \geq 6$), the thickness of the ocean layer is reduced to < 2.5 times the wavelength, because of computational limits for large meshes. The planar meshes we implement do not include support from membrane stresses, which becomes appreciable when the horizontal scale of a comparable spherical harmonic degree is roughly the same as the square root of the planetary radius divided by the lithospheric thickness (Turcotte, 1981). For Europa, this corresponds to a spherical harmonic degree of ~16 (~600 km). As will be discussed in subsequent sections, the additional support provided by membrane stress simply adds to the already sufficient support to maintain topography at those wavelengths.

Elements in our mesh are uniformly distributed in the ice shell and concentrated towards the ice-ocean boundary in the ocean layer, while remaining below a 4:1 aspect ratio. Mesh resolution is variable depending on the scale of the wavelength. At the smallest scales, the ice portion of the mesh has, at minimum, 400 finite elements (40 in depth and 10 in width). At the largest scales, this ratio is reversed to keep within the 4:1 aspect ratio, with 400 elements in width and 10 in depth. Free-slip conditions are applied to the symmetry boundaries at the sides of the mesh, restricting normal displacements, and the bottom of the mesh is locked horizontally and vertically. On the surface, we place sinusoidal topography with an amplitude h of 100 m for all wavelengths, as wavelength controls buoyant support rather than topographic amplitude (see

Turcotte & Schubert, 2014). We simulate two scenarios for initial topography at the base of the ice shell: 1) a flat basal surface (i.e., no initial compensating topography), and 2) a root in isostatic equilibrium. The maximum amplitude of the isostatic root H is determined by the density contrast between the water ice and ocean where

$$H = \frac{\rho_i h}{\rho_w - \rho_i}. \quad (1)$$

In this equation, the density of the liquid water ρ_w is assumed to be 1000 kg/m^3, while the density of the ice shell ρ_i is 920 kg/m^3. Gravitational body forces are applied uniformly to the mesh with an acceleration equal to 1.315 m/s^2.

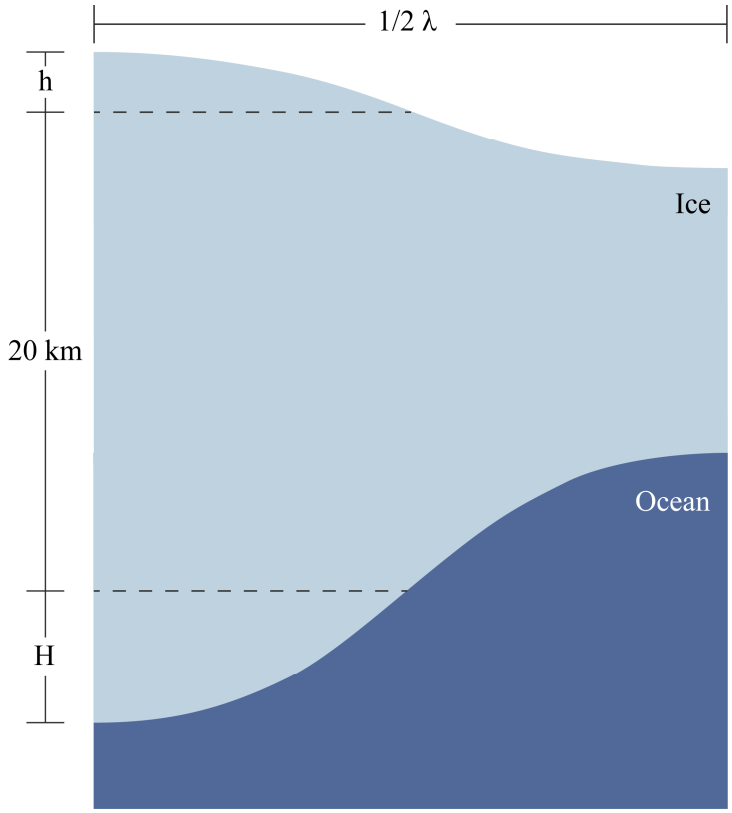

Figure 1. Schematic of basic model setup using an ice shell assuming an initial state of isostasy. The amplitude h is 100 m for all models regardless of wavelength resulting in an amplitude for basal topography H of 1150 m.

2.3 Material and thermal properties

The elastic parameters for ice include a Young's modulus of 9.32 GPa and a Poisson ratio of 0.325 (Gammon et al., 1983). However, in simulations, applying a gravitational load to a compressible material leads to deviatoric stresses from self-compaction. Following Dombard and

McKinnon (2006b), we make the material nearly incompressible by adjusting the Poisson ratio to approach 0.5, while also reducing the Young's modulus to 7.83 GPa as to maintain the flexural rigidity of the ice. The viscosity structure of the ice layer has the greatest influence on relaxation rates (Dombard & McKinnon, 2006a), and when incompressibility is approximated, the variation is negligible.

Additionally, we follow the ductile creep laws from Goldsby and Kohlstedt (2001). Several mechanisms affect the viscous flow of ice below the brittle-ductile transition. There are three different dislocation (dis) creep mechanisms with temperature dependent contributions (Durham & Stern, 2001), diffusion (diff) creep; and dislocation in an easy-slip (ES) system and grain boundary sliding (GBS) acting as rate limiters. Thus, the total strain rate is

$$\dot{\epsilon}_{total} = \dot{\epsilon}_{dis} + \dot{\epsilon}_{diff} + \left(\frac{1}{\dot{\epsilon}_{ES}} + \frac{1}{\dot{\epsilon}_{GBS}}\right)^{-1}. \quad (2)$$

Each of these strain rates can take the general form

$$\dot{\epsilon} = A\left(\frac{1}{d}\right)^{m} \sigma' e^{-\left(\frac{Q}{RT}\right)}, \quad (3)$$

where $\dot{\epsilon}$ is the equivalent strain rate, A is a material dependent pre-exponential constant normalized for uniaxial deformation, m is a grain size index relating to the grain size d, Q is the activation energy, R is the universal gas constant, and T is absolute temperature. We assume a grain size of 1 mm (e.g., Dombard & McKinnon, 2006a). The full creep parameters are listed in Durham et al. (2010) and references therein.

The thermal conductivity of water ice is temperature dependent, given by $651/T$ (Petrenko & Whitworth, 1999). In our steady state thermal simulation, we lock the surface temperature at 100 K and the ice-ocean interface temperature at the melting point of ice, 273 K ($q \approx 32$ mW/m^3). Heat flows on Europa might be higher, instigating convection near the base of the shell (e.g., McKinnon, 1999; Tobie et al., 2003). Nonetheless, for our purposes, the situation is mechanically identical: a structurally weak base overlaid by a relatively thinner lithosphere (see below).

The water below the ice shell lacks material strength and therefore does not provide resistance; rather, it provides a buoyant restoring force. The viscosity is so low compared to the lithospheric ice in the upper shell that it simply needs to accommodate space for the deforming

ice at least as fast as that ice is deforming. Therefore, we set the material properties of the water to be the same as the overlying ice layer, with the exception of the density contrast. We also test for the effects of surface temperature, which have been shown to be a controlling factor in creep rates (e.g., Damptz & Dombard., 2011), and the effects for a reduction in the melting temperature of ice due to the presence of an antifreeze such as ammonia (e.g., Spohn & Schubert, 2003). To test for effects of buoyancy, we run the simulations without the density contrast, precluding isostasy. Variations in model parameters are shown in Supporting Information Table S1.

We run the simulations for 3 Gyr, a time more than sufficient to capture any appreciable flow in the lower ice shell. Time steps are controlled by the minimum Maxwell time, which is dependent upon, in part, the viscosity (Turcotte & Schubert, 2014). We limit minimum viscosity in the mesh to 10^{18}Pa s, keeping run times reasonable, and confirm that our results are not sensitive to viscosity cutoffs below this value.

Simulations are performed under full large-strain formulation, which includes a second-order term to strain-displacement relationships (e.g., Ranalli, 1995), and a continual geometric update. Although strains are typically small, the large strain scheme is essential for the geometric update, as without it, stresses would not decay as topography relaxes (e.g., Dombard & McKinnon, 2006a). In addition, we apply constant dilatation across the elements to eliminate potential numerical errors caused by simulating a nearly incompressible material.

3 Results

The evolution of topography can be described best by three general wavelength categories: short, intermediate, and long. Figure 2 shows the simulation results for the evolution of topography at the surface and base of the ice shell for three representative wavelengths within these categories.

At short wavelengths, the surface topography remains stable over the simulation time regardless of buoyancy. In contrast, the basal topography relaxes away, losing 991 m of its initial amplitude. For intermediate wavelengths, the surface topography relaxes in both the buoyancy and no buoyancy simulations. However, the degree of relaxation is substantially greater when the density contrast is not present. For instance, for a wavelength of 100 km, the surface loses approximately 65% of its elevation over the simulation time, compared to an 85% loss for the

no-buoyancy scenario (Figure 2c). The root topography at intermediate wavelengths also relaxes when the density contrast is present. Moreover, it relaxes at a rate out of isostatic equilibrium with the relaxation of the surface topography (Figure 2d), resulting from the shared contribution of both lithospheric support and buoyancy (Figure 3a).

In the case of long wavelengths, without the density contrast, the surface completely relaxes away in less than 100 kyr. Conversely with the density contrast, the surface and the root are stable over geologic times.

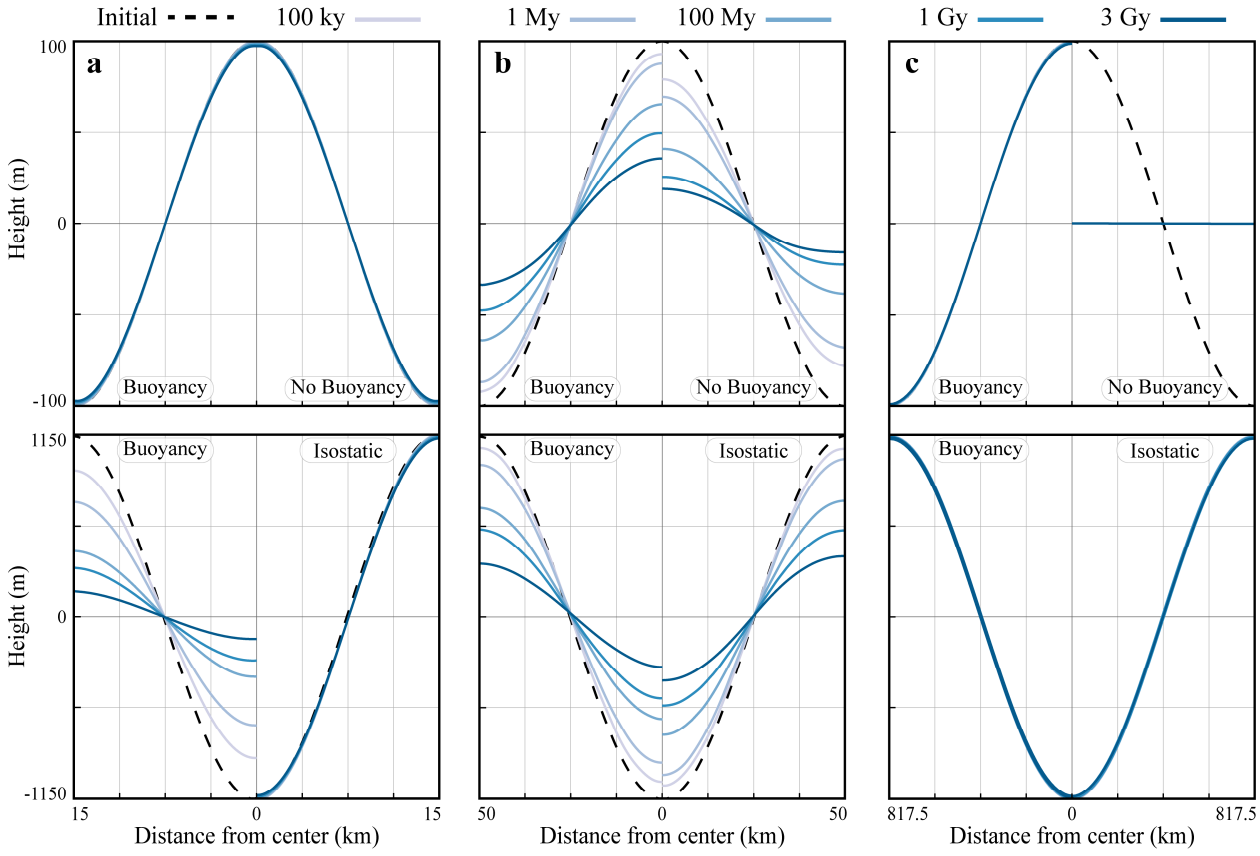

Figure 2. Simulation results for the surface topography (top row) and root topography (bottom row) for wavelengths of a) 30 km, b) 100 km, and c) 1635 km (spherical harmonic degree $l \approx 6$). The initial topography (black dashed line) is the same for each model, sinusoidal with an amplitude of 100 m for the surface topography and 1150 m for the root topography. For the surface topography, the left side of $x = 0$ are simulations with an ice-ocean density contrast (i.e., buoyancy), and the right side of $x = 0$ are the simulations without the density contrast (i.e., no buoyancy). For the root topography, the left side of $x = 0$ are the simulations with the density contrast (i.e., buoyancy), and the right side of $x = 0$ are the expected isostatic root topography given by equation (1) assuming the surface of the buoyancy simulations (top row, left side of x-axes). Because the buoyancy simulations are set up to be in isostatic equilibrium, the results should be static if the precepts of Airy isostasy hold.

Simulations with a surface temperature of 100 K show that the lithosphere supports the topographic load up to wavelengths of ~30 km (Figure 3). Lowering the surface temperature increases the wavelengths at which lithospheric strength can effectively contribute to topographic support. A decreased surface temperature also reduces the degree of relaxation occurring at intermediate wavelengths. For example at 100 km, the simulated surface topography with temperatures of 100 K relax ~65 m, compared to ~15 m when the surface temperature is 70 K. A similar effect is observed when the melting temperature (i.e., the temperature at the ice-ocean interface) is reduced to 176 K (Figure 3b). Under these conditions, the contribution of lithospheric support is greater at longer wavelengths, and the maximum topographic relaxation is reduced.

At wavelengths < 80 km, the simulations with the base of the ice shell initially flat is nearly identical to that with the simulations without the density contrast. This finding further underscores that lithospheric strength is the primary mechanism of topographic support at short wavelengths. However, at wavelengths greater than 100 km, without an initial compensated root, the surface topography relaxes to just a few meters over the simulated time. At the longest wavelengths, a root forms that is in isostatic equilibrium with the reduced surface topography.

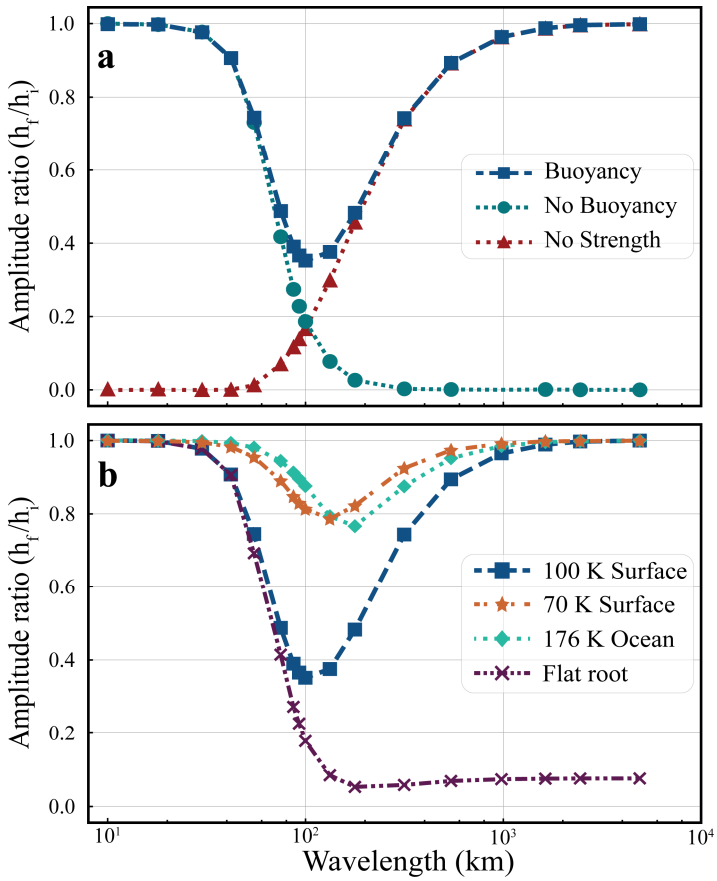

Figure 3. Ratio of initial to final topographic amplitude for simulations across simulated wavelengths for a) simulations with and without buoyancy and b) variations in the assumed initial state of the temperature at the surface and base of the ice shell. Because the simulations (except the "Flat root" ones) are set up to be in isostatic equilibrium, the ratio should be pegged to a value of 1 if the precepts of Airy isostasy hold; i.e., Airy isostasy fails when the amplitude ratio is < 1.

4 Discussion

The prevalent assumption that Airy isostasy can be utilized for estimating ice shell thickness does not hold true except at the longest wavelengths. A significant oversight in this assumption lies in the positioning of the lithosphere relative to the ice-ocean boundary. On Earth, the lithospheric boundary is situated beneath the density contrast of the crust-mantle boundary. Thus, when a surface load deforms the lithosphere, both the crust and the upper mantle will respond to the deformation (e.g., Barrell, 1914; Daly, 1940). However, in the case of ice shells, the lithosphere is embedded within the ice itself, because the ice in the lower portion of the shell is approaching its melting point and is therefore weak over geologic time scales. (A convective portion in an ice shell that passes a higher heat flux would only exasperate this effect.)

Our findings also illustrate that the lithosphere of ice shells can support topographic loads at short wavelengths. The short-wavelength scenario shows surface topography to be stable with and without buoyancy, while the initially isostatic basal topography relaxes away (Figure 2a), indicating that contribution of buoyancy supporting the load is insignificant and that any root sticking into the ocean would flow away rapidly. The length at which lithospheric support begins to decrease is contingent on the surface temperature, and potentially, the presence of antifreeze in the ocean. These findings agree with Damptz and Dombard (2011), who highlighted the significant role of surface temperature in controlling creep at the base of the lithosphere for the moons of Jupiter and Saturn. Due to viscous creep, the lithosphere is not static. Stresses relax at the base of the lithosphere, allowing the lithosphere to thin with time. Surface temperature, and to a lesser degree heat flow and grain size, control creep rates.

It is important to note that while the surface topography at both short and long wavelengths can be stable over geologic times, the basal topography exhibits distinctly different behaviors at varying spatial scales. At short wavelengths, basal topography relaxes away indicating topographic features at these scales are not compensated. Conversely, at long wavelengths, topography at the base of the ice shell stays in isostatic equilibrium with the surface topography. This finding can be attributed to the relative size of the vertical flow region and the lateral extent of the topography. For long wavelengths, the vertical extent of the area where material can flow laterally and redistribute is small compared to the horizontal extent (cf. Stevenson, 2000). This imbalance results in a highly channelized flow that inhibits the overall relaxation process observed at shorter wavelengths.

Moreover, when the wavelength of a load is small compared to the planetary radius, the stresses caused by the body's curvature can be ignored. However, when curvature is introduced, horizontal membrane stresses can contribute to the support of the surface load (Turcotte, 1981). In the context of this study, membrane stresses are appreciable at approximately spherical harmonic degree $l = 16$, assuming the lithosphere is ~6 km thick. This degree corresponds to a wavelength of ~600 km. At this scale, topography loses just 10% of its initial height when surface temperature is 100 K, and this relaxation is further reduced for colder surface temperatures (Figure 3). Consequently, the inclusion of membrane stresses would reinforce our findings regarding the stability of long wavelength topography.

To sum up, there are two competing effects for the application of Airy isostasy in an ice shell over an ocean, one of which does not exist in traditional applications of Airy isostasy in terrestrial worlds. First, the lithospheric strength of icy shells is a sufficient support mechanism for topography at short wavelengths, without needing help from buoyancy. This finding is evidenced by the "No buoyancy" curve in Figure 3a, and it mirrors the lithospheric behavior of rocky planets. In contrast, the "No strength" curve in Figure 3a, which does not come from simulations but from subtracting the "Buoyancy" and "No buoyancy" curves and thus mimics a scenario where any lithosphere would have no strength, stands in contrast to the expected behavior in a terrestrial world, which would be locked at 1 at all scales. These two curves – "No buoyancy" and "No strength" – together determine the final topographic support.

To understand this behavior, consider the effect of pressing one's finger into a seat cushion. The cushion diffuses the stresses introduced by the force of the finger, and the opposite side of the cushion is negligibly deformed, if at all. A sufficiently wide scale load, however, would feel the hard seat underneath, even when pressed into the cushion at the same force per unit area. Translating to ocean worlds, the seat cushion inhibits buoyant support at short wavelengths, though the lithosphere can provide the support, while concurrent, the basal topography can relax away without affecting the surface. At long wavelengths, the seat cushion is too thin for buoyancy to be inhibited, so topography can be supported, even if the lithosphere provides no support. Simultaneously at these scales, highly channelized flow precludes relaxation of the basal topography. At intermediate scales, neither the seat cushion or the lithosphere are fully effective, and topography cannot be supported over geologic timescales by a crustal root alone, and would need another mechanism of support (e.g., Pratt). How these curves add, and thus the size of the intermediate zone, is dependent on local conditions, as suggested by Figure 3b. For the case of Europa explored here, this wavelength range spans over an order of magnitude (from < 100 km to > 1000 km), with substantial lack of support for equatorial regions where surface temperatures are higher.

4 Conclusion

Our results yield a more nuanced understanding of the wavelength dependence of icy shell evolution, offering insights that could enhance the interpretation of topography and gravity data from the icy, ocean worlds. While surface topography of short-wavelength features persists

over geologic time, compensated roots relax away quickly. Consequently, shell thickness estimates derived from short-wavelength features will not accurately represent the local thickness. In contrast, long-wavelength topography could be supported by shell thickness variations, such as on Titan (Nimmo and Bills, 2010). Surface topography at intermediate scales is unlikely to be isostatically compensated via buoyant support.

The practical implications of this more complex behavior has already been revealed at other icy worlds. The isolated plateaus on Titan appear to exist in the short wavelength regime, being supported by the strength of Titan's lithosphere with any root relaxing away quickly, suggesting top-down construction of the plateaus (Schurmeier et al., 2016). Conversely, the megadome on Ganymede appears to be firmly in the intermediate regime, unable to be supported by either lithospheric strength of a buoyant crustal root and implicating Pratt isostasy (Kay et al., 2018).

Such complexities and limitations underscore the challenges inherent in applying traditional isostatic models to icy shells and highlight the importance of continuous model refinement. Furthermore, the importance of a nuanced understanding of the dynamics of icy shells cannot be overstated, especially in the context of future space missions.

Acknowledgments

This work was supported in part by NASA through the Europa Clipper Project, via JPL subcontract 1656601.

Open Research

The Marc software is available from https://hexagon.com/products/marc; academic pricing is available. Supporting information Table S2 shows the elevations of the surface and root topographies, calculated from displacements, for each simulation type and wavelength. A csv file of Table S2 is available at https://doi.org/10.5281/zenodo.8277281 (Tucker & Dombard, 2023).

References

Airy, G. B. (1855). On the computation of the effect of the attraction of mountain-masses, as disturbing the apparent astronomical latitude of stations in geodetic surveys. *Philosophical Transactions of the Royal Society of London*, *145*, 101–104. https://doi.org/10.1098/rstl.1855.0003

Barrell, J. (1914). The Strength of the Earth's Crust. *The Journal of Geology*, *22*(8), 729–741. https://doi.org/10.1086/622189

Beuthe, M. (2021a). Isostasy with Love – I: elastic equilibrium. *Geophysical Journal International*, *225*(3), 2157–2193. https://doi.org/10.1093/gji/ggab073

Beuthe, M. (2021b). Isostasy with Love: II Airy compensation arising from viscoelastic relaxation. *Geophysical Journal International*, *227*(1), 693–716. https://doi.org/10.1093/gji/ggab241

Billings, S. E., & Kattenhorn, S. A. (2005). The great thickness debate: Ice shell thickness models for Europa and comparisons with estimates based on flexure at ridges. *Icarus*, *177*(2), 397–412. https://doi.org/10.1016/j.icarus.2005.03.013

Čadek, O., Souček, O., & Běhounková, M. (2019a). Is Airy Isostasy Applicable to Icy Moons? *Geophysical Research Letters*, *46*(24), 14299–14306. https://doi.org/10.1029/2019GL085903

Čadek, O., Souček, O., Běhounková, M., Choblet, G., Tobie, G., & Hron, J. (2019b). Long-term stability of Enceladus' uneven ice shell. *Icarus*, *319*(May 2018), 476–484. https://doi.org/10.1016/j.icarus.2018.10.003

Damptz, A. L., & Dombard, A. J. (2011). Time-dependent flexure of the lithospheres on the icy satellites of Jupiter and Saturn. *Icarus*, *216*(1), 86–88. https://doi.org/10.1016/j.icarus.2011.07.011

Dahlen, F. A. (1982). Isostatic geoid anomalies on a sphere. *Journal of Geophysical Research*, *87*(B5), 3943. https://doi.org/10.1029/JB087iB05p03943

Daly, R. A. (1940). *Strength and structure of the Earth*. Hinds, N. (Ed.). New York, NY: Prentice-Hall.

Dombard, A. J., & McKinnon, W. B. (2000). Long-term retention of impact crater topography on Ganymede. *Geophysical Research Letters*, *27*(22), 3663–3666. https://doi.org/10.1029/2000GL011695

Dombard, A. J., & McKinnon, W. B. (2006a). Elastoviscoplastic relaxation of impact crater topography with application to Ganymede and Callisto. *Journal of Geophysical Research: Planets*, *111*(1), 1–22. https://doi.org/10.1029/2005JE002445

Dombard, A. J., & McKinnon, W. B. (2006b). Folding of Europa's icy lithosphere: an analysis of viscous-plastic buckling and subsequent topographic relaxation. *Journal of Structural Geology*, *28*(12), 2259–2269. https://doi.org/10.1016/j.jsg.2005.12.003

Durham, W. B., Prieto-Ballesteros, O., Goldsby, D. L., & Kargel, J. S. (2010). Rheological and Thermal Properties of Icy Materials. *Space Science Reviews*, *153*(1–4), 273–298. https://doi.org/10.1007/s11214-009-9619-1

Durham, W. B., & Stern, L. A. (2001). Rheological properties of water ice—Applications to satellites of the outer planets. *Annual Review of Earth and Planetary Sciences*, *29*(1), 295–330. https://doi.org/10.1146/annurev.earth.29.1.295

Gammon, P. H., Kiefte, H., & Clouter, M. J. (1983). Elastic constants of ice samples by Brillouin spectroscopy. *The Journal of Physical Chemistry*, *87*(21), 4025–4029. https://doi.org/10.1021/j100244a004

Goldsby, D. L., & Kohlstedt, D. L. (2001). Superplastic deformation of ice: Experimental observations. *Journal of Geophysical Research: Solid Earth*, *106*(B6), 11017–11030. https://doi.org/10.1029/2000JB900336

Hemingway, D. J., & Matsuyama, I. (2017). Isostatic equilibrium in spherical coordinates and implications for crustal thickness on the Moon, Mars, Enceladus, and elsewhere. *Geophysical Research Letters*, *44*(15), 7695–7705. https://doi.org/10.1002/2017GL073334

Hussmann, H., Spohn, T., & Wieczerkowski, K. (2002). Thermal equilibrium states of Europa's ice shell: Implications for internal ocean thickness and surface heat flow. *Icarus*, *156*(1), 143–151. https://doi.org/10.1006/icar.2001.6776

Kay, J. P., & Dombard, A. J. (2018). Formation of the bulge of Iapetus through long-wavelength folding of the lithosphere. *Icarus*, *302*, 237–244. https://doi.org/10.1016/j.icarus.2017.10.033

Kay, J. P., Schenk, P. M., Dombard, A. J., & McKinnon, W. B. (2018). The 3-km high subjovian megadome on Ganymede: Simulation of stability via Pratt isostasy. In *49th Lunar and Planetary Science Conference*.

McKinnon, W. B. (1999). Convective instability in Europa's floating ice shell. *Geophysical Research Letters*, *26*(7), 951–954. https://doi.org/10.1029/1999GL900125

Nimmo, F., & Bills, B. G. (2010). Shell thickness variations and the long-wavelength topography of Titan. *Icarus*, *208*(2), 896–904. https://doi.org/10.1016/j.icarus.2010.02.020

Nimmo, F., Bills, B. G., & Thomas, P. C. (2011). Geophysical implications of the long-wavelength topography of the Saturnian satellites. *Journal of Geophysical Research: Planets*, *116*(11), 1–12. https://doi.org/10.1029/2011JE003835

Nimmo, F., Giese, B., & Pappalardo, R. T. (2003a). Estimates of Europa's ice shell thickness from elastically-supported topography. *Geophysical Research Letters*, *30*(5), 1–4. https://doi.org/10.1029/2002gl016660

Nimmo, F., Pappalardo, R. T., & Giese, B. (2003b). On the origins of band topography, Europa. *Icarus*, *166*(1), 21–32. https://doi.org/10.1016/j.icarus.2003.08.002

Ojakangas, G. W., & Stevenson, D. J. (1989). Thermal State of an Ice Shell on Europa. *Icarus*, *81*(2), 220–241. https://doi.org/10.1016/0019-1035(89)90052-3

Pappalardo, R. T., Belton, M., Breneman, H. H., Carr, M. H., Chapman, C. R., Collins, G. C., et al. (1999). Does Europa have a subsurface ocean? Evaluation of the geological evidence. *Journal of Geophysical Research: Planets*, *104*(E10), 24015–24055. https://doi.org/10.1029/1998JE000628

Petrenko, V. F., & Whitworth, R. W. (1999). *Physics of Ice*. *Physics of Ice*. Oxford University Press. https://doi.org/10.1093/acprof:oso/9780198518945.001.0001

Pratt, J. H. (1855). On the attraction of the Himalaya Mountains, and of the elevated regions beyond them, upon the plumb-line in India. *Philosophical Transactions of the Royal Society of London*, *145*(2), 53–100. https://doi.org/10.1098/rstl.1855.0002

Prockter, L. M., Patterson, G. W. (2009). Morphology and Evolution of Europa's Ridges and Bands. In R. T. Pappalardo, W. B. McKinnon, & K. K. Khurana (Eds.), *Europa* (pp. 237–258). University of Arizona Press. https://doi.org/10.2307/j.ctt1xp3wdw.16

Ranalli, G. (1995). *Rheology of the Earth*. Chapman and Hall.

Schenk, P. M., & McKinnon, W. B. (2009). One-hundred-km-scale basins on Enceladus: Evidence for an active ice shell. *Geophysical Research Letters*, *36*(16), 1–5. https://doi.org/10.1029/2009GL039916

Schmidt, B. E., Blankenship, D. D., Patterson, G. W., & Schenk, P. M. (2011). Active formation of "chaos terrain" over shallow subsurface water on Europa. *Nature*, *479*(7374), 502–505. https://doi.org/10.1038/nature10608

Schurmeier, L. R., Dombard, A. J., & Radebaugh, J. (2016). Titan's isolated mountain plateaus: Investigating possible support mechanisms and cryovolcanic origins. In *47th Lunar and Planetary Science Conference*.

Spohn, T., & Schubert, G. (2003). Oceans in the icy Galilean satellites of Jupiter? *Icarus*, *161*(2), 456–467. https://doi.org/10.1016/S0019-1035(02)00048-9

Stevenson, D. J. (2000). Limits on the variation of thickness of Europa's ice shell. In *31st Lunar and Planetary Science Conference*.

Tobie, G., Choblet, G., & Sotin, C. (2003). Tidally heated convection: Constraints on Europa's ice shell thickness. *Journal of Geophysical Research*, *108*(E11), 5124. https://doi.org/10.1029/2003JE002099

Tucker, W. S., & Dombard, A. J. (2023) Elevation data for On the More Complex Wavelength Dependency of Airy Isostasy in Icy Shells of Ocean Worlds [Data set]. Zenodo. https://doi.org/10.5281/zenodo.8277281

Turcotte, D. L., & Schubert, G. (2014). *Geodynamics*. Cambridge University Press.

Turcotte, D. L., Willemann, R. J., Haxby, W. F., & Norberry, J. (1981). Role of membrane stresses in the support of planetary topography. *Journal of Geophysical Research*, *86*(B5), 3951–3959. https://doi.org/10.1029/JB086iB05p03951

Williams, K. K., & Greeley, R. (1998). Estimates of ice thickness in the Conamara Chaos Region of Europa. *Geophysical Research Letters*, *25*(23), 4273–4276. https://doi.org/10.1029/1998GL900144